Surface Chemistry of Ultrathin Films of Histidine on Gold As Probed by High-Resolution Synchrotron Photoemission

Yan Zubavichus,*,†,‡ Michael Zharnikov,† Yongjie Yang,† Oliver Fuchs,§ Clemens Heske,|| Eberhard Umbach,§ George Tzvetkov,⊥ Falko P. Netzer,⊥ and Michael Grunze†

Angewandte Physikalische Chemie, University of Heidelberg, INF 253, 69120 Heidelberg, Germany, Institute of Organoelement Compounds, Russian Academy of Sciences, 28 Vavilova Street, 119991 Moscow, Russia, Experimentelle Physik II, University of Würzburg, Am Hubland, 97074 Würzburg, Germany, Department of Chemistry, University of Nevada, 4505 Maryland Parkway, Las Vegas, Nevada 89154-4003, and Institut für Experimentalphysik, Karl-Franzens-Universität Graz, Universitätsplatz 5, 8010 Graz, Austria

Received: June 2, 2004; In Final Form: October 21, 2004

Procedures for the vacuum deposition of thin histidine films on polycrystalline Au(111) and their characterization with high-resolution synchrotron-radiation-based photoelectron spectroscopy are reported. The chemical form of histidine (anionic vs zwitterionic) and the nature of its interactions with the substrate (strong ionic−covalent vs weak van der Waals bonding) in mono- and multilayer films are analyzed. It is shown that water adsorption on a pre-prepared histidine film at 100 K results in protonation of histidine molecules and partial formation of hydroxyl anions. These chemical effects are carefully differentiated from spectral changes associated with radiation damage of the histidine films.

1. Introduction

Bioorganic interfaces are of great interest in many fields ranging from medicine to nanotechnology.[1] Among them, adsorbates of amino acids on noble metals may be considered as some of the simplest reference systems. In general, there are two routine ways to produce thin overlayers of amino acids on specific substrates: adsorption from solution and vacuum deposition. Systematic studies of amino acids deposited onto various surfaces (noble metals, silicon, graphite, etc.) from diluted aquatic solutions near the isoelectric point have been conducted since the mid 1980s.[2−6] Films of amino acids deposited onto metallic surfaces under ultrahigh vacuum (UHV) conditions have also been investigated.[7−15] However, there is a serious problem with the latter approach because the saturation vapor pressure of many amino acids is extremely low even at temperatures close to their decomposition temperature. This is due to the zwitterionic nature of amino acids in the solid state, resulting in the formation of strong intermolecular bonds. Zwitterionic amino acids are similar in some respects to organic polymers (for instance, most amino acids melt above 250 °C and only with progressive decomposition). Therefore, most vacuum-deposition studies have been focused on the simplest and smallest amino acids, such as glycine, alanine, and cysteine.

In this work, we report on the vacuum deposition of a relatively large amino acid, histidine, onto a polycrystalline gold substrate. To our knowledge, no studies using vacuum deposition of this amino acid have been reported so far. The molecular formula of histidine is shown in Figure 1. Among the 20 naturally occurring amino acids, histidine is unique. In addition to amino and carboxyl groups, which are common to all amino acids, it contains an imidazole ring, which strongly affects its chemical properties. For most amino acids, acid−base equilibria in aqueous solutions include four species: cationic, zwitterionic, neutral (molecular), and anionic. For histidine, the number of such species is even larger due to the additional possibilities of protonation or deprotonation of the imidazole ring, as shown in Figure 2.[16,17] Both protonation of the pyridine-like N_3 atom and deprotonation of the pyrrole-like N_1 atom within the imidazole moiety retain the aromaticity of the heterocycle and result in two chemically equivalent nitrogen atoms.

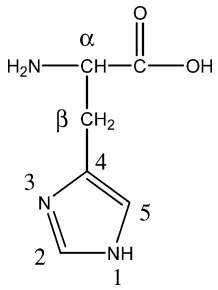

Figure 1. Molecular formula of histidine and numeration of atoms therein.

Apart from these acid−base properties, the imidazole ring has a high coordination affinity toward transition metals.[18] Coordination of a histidine residue to transition metals is found in many important metalloenzymes, such as hemoglobin and myoglobin. Many complexes of histidine with transition metals have been prepared as single crystals and structurally characterized with X-ray diffraction techniques. Histidine may be coordinated to metal atoms via amino groups, carboxyl groups, or the nitrogen atoms of the imidazole ring, thus acting as a mono-,[19] bi-,[20,21] or tridentate[22] ligand. A few histidine−gold complexes have been described and characterized spectroscopically or electrochemically,[23,36] but no X-ray crystallographic studies have been reported to date. In the crystal

* To whom correspondence should be addressed: e-mail yan.zubavichus@urz.uni-heidelberg.de.
† University of Heidelberg.
‡ Russian Academy of Sciences.
§ University of Würzburg.
|| University of Nevada.
⊥ Karl-Franzens-Universität Graz.

10.1021/jp047626m CCC: $30.25
Published on Web 12/03/2004

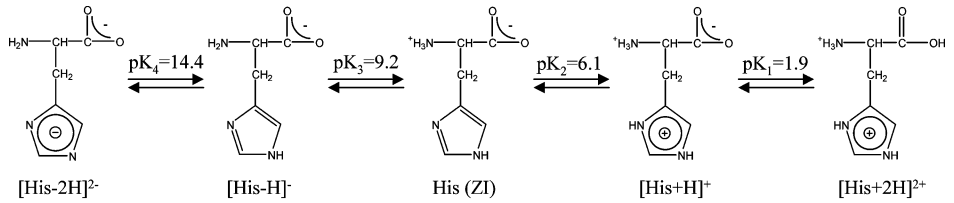

Figure 2. Ionic species of histidine present in aqueous solutions at different pH values and respective equilibrium constants.

TABLE 1: Parameters for Preparation of Ultrathin Histidine Films on Gold

	film 1	film 2	film 3
evaporator temperature, °C	105	115	115
substrate temperature	RT	RT	RT
deposition time, min	40	40	80
estimated film thickness, Å (±10%)	5.2	18.5	38.8

structure of a gold(III) complex with a related ligand, glycyl-histidine, three nitrogen atoms of the dipeptide (N_3 atom of the imidazole ring, amido N of the peptide bridge, and N of the amino group) were found to be involved in the coordination to gold atoms.[25] Recently, a coordination of a histidine residue to gold(I) has been revealed in the crystal structure of a gold complex with the protein cyclophilin.[26] It is noteworthy that this coordination type is realized despite the availability of several thiolate moieties in the protein, thus demonstrating a high affinity of gold atoms toward histidine.

Multilayers of histidine on gold prepared by adsorption from aqueous solutions near the isoelectric point have been studied by Liedberg et al.[27] by means of infrared reflection−absorption spectroscopy. They found that the zwitterionic histidine forms only weak van der Waals bonds to gold, whereas in a similarly prepared copper derivative, the bonding (suggested to involve amino and carboxyl groups) was strong and substantially covalent.

The aim of this study is therefore to elucidate the chemical identity and adsorption geometry of the histidine in ultrathin films prepared by vacuum deposition on polycrystalline gold. Taking into account that histidine residues play a dominant role in the protein−metal binding, this information is crucial for the design of efficient protein-processing devices, for example, for protein separation, immobilization, or detection.[28,29]

2. Experimental Section

In the present study, commercially available polycrystalline powder of L-histidine (Sigma−Aldrich, purity >98%) was used. The vacuum deposition of histidine was performed using a Knudsen cell-type evaporator in a UHV chamber with a base pressure better than 8×10^{-10} Torr. Before the deposition, the histidine powder was carefully degassed in a vacuum at 70 °C. Three films of histidine with different thicknesses were produced under the preparation conditions listed in Table 1. As a substrate, polycrystalline Au-covered silicon wafers (15×15 mm^2) with the preferential (111) orientation of crystallites were used. Prior to the deposition, the substrates were thoroughly cleaned by Ar^+ sputtering (kinetic energy 1.5 kV, incidence angle 45°), followed by annealing at 700 °C.

High-resolution X-ray photoelectron spectroscopy (XPS) measurements were performed at the UE52-PGM undulator beamline of the BESSY II storage ring in Berlin, which is equipped with a plane-grating monochromator (PGM), a Scienta SES200 hemispherical electron energy analyzer, and a multichannel plate detector. The photon beam was incident at 55° relative to the surface normal, and the spectra were recorded in normal emission geometry. Photon energies of 720, 610, and 160 eV were used to measure survey spectra, narrow scans in the regions of C 1s/N 1s/O 1s/Au 4f core levels, and valence band spectra, respectively. The pass energy was set to 75 eV for the survey spectra and to 40 eV for the core level spectra. For the latter, the combined monochromator−analyzer energy resolution was between 110 meV ($h\nu = 160$ eV) and 140 meV ($h\nu = 610$ eV), as determined from the widths of the Au Fermi edges measured on a freshly sputtered gold sample. This edge was also used as a calibration point for the energy scale. For processing the C 1s, N 1s, and O 1s spectra, a polynomial background and symmetric Gaussian peak functions were used, while the Au 4f spectra were analyzed by use of a Shirley background and Pearson VII peak functions. Reference low-resolution XPS spectra of histidine polycrystalline powder were measured on a laboratory ESCAscope spectrometer (Mg Kα excitation) as described elsewhere.[30]

In general, unexposed spots on the sample were selected for each new measurement (the size of the beam spot on the sample is estimated to be 0.8×0.2 mm^2). On average, the acquisition of a single XPS spectrum took about 2 min. To monitor spectral changes due to radiation damage, 8−10 consecutive scans on the same spot were collected. To account for a dependence of the damage rate on the beam flux, the actual beam exposure times were normalized to the storage ring current so that equivalent exposure times, corresponding to an exposure at the mean storage ring current of 100 mA, are referenced to in the paper. Under these conditions, the photon flux is estimated to be 3×10^{11} photons/s.

The spectroscopic characterization of the histidine films was performed at room temperature. In addition, water adsorption onto the evaporated histidine films was studied in order to elucidate the impact of ambient conditions on the electronic structure of the histidine films. For these measurements, the predeposited histidine sample was cooled to 100 K in UHV. Since, according to the mass-spectral analysis, water (m/e peak at 18 AMU) was by far the dominant component of the residual vacuum in the analysis chamber, this effectively corresponds to a deliberate exposure to water molecules. No evidence for the adsorption of other gaseous species from the residual gas (CO, CO_2, etc.) was found. The water uptake was quantified from the O 1s XPS data. In parallel, water exposures were calculated by use of 3×10^{-10} Torr as an estimate of the partial water vapor pressure. The ensuing XPS measurements were performed at 100 K as well.

3. Results and Discussion

3.1. Preparation and Characterization of Pristine Histidine Films. Survey XPS spectra of the pristine histidine films 1−3 and after specific treatments (to be discussed below) are shown in Figure 3. The photoemission peaks corresponding to Au, C, N, and O are easily identifiable. In the series film 1−film 2−film 3, the film thickness increases as seen from the intensities of the C, N, and O peaks relative to that of Au.

XPS spectra in the regions of Au 4f, O 1s, N 1s, and C 1s core levels together with the peak-fitting results are shown in

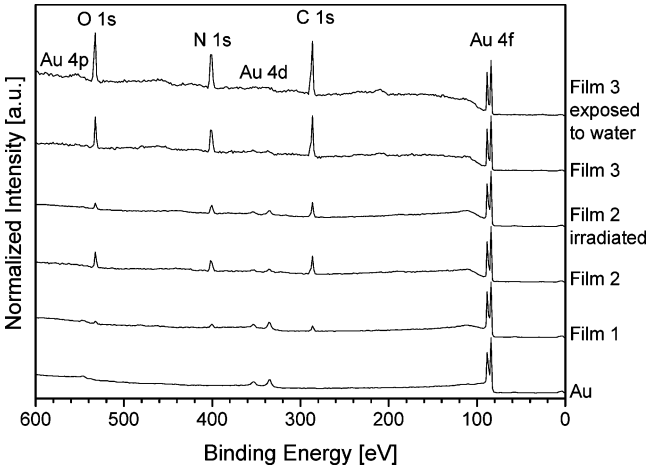

Figure 3. Survey spectra ($h\nu = 720$ eV) of clean gold, pristine histidine films 1−3, histidine film 2 exposed to soft X-ray irradiation, and histidine film 3 exposed to the UHV environment for 200 min at 100 K.

Figure 4. For better comparison, the top row shows the spectra normalized to the maximum intensity and offset vertically. The bottom row shows the identical spectra, but normalized to the storage ring current, which thus allows a direct comparison of the absolute experimental intensities. The Au emission intensity of films 1−3 (first panel of Figure 4) decreases with respect to clean gold due to attenuation by the histidine layers. Assuming a homogeneous histidine film (for justification, see below), this attenuation allows an estimate of the film thickness according to the standard formula $I_d = I_0 \cdot \exp(-\lambda/d)$ where d is the thickness of the organic overlayer, I_d is the intensity of the signal from the substrate attenuated by the overlayer, I_0 is the intensity of the signal measured for the clean substrate, and λ is the inelastic electron mean-free path. The latter value was approximated as $\lambda = 0.272E_{kin}^{0.67}$, where E_{kin} is the kinetic energy of the detected photoelectrons.[31,32] The accuracy of this procedure is ca. 10%.

The film thicknesses obtained in this way are given in Table 1. For film 1, the effective thickness is estimated to be 5.2 Å. This value is close to the minimum dimension of a histidine molecule, which suggests that the film cannot be much thicker than one monolayer. Note that the effective thicknesses of films 2 (18.5 Å) and 3 (38.8 Å), which were deposited at the same evaporator temperature of 115 °C, are approximately proportional to the deposition time. We assume that both films 2 and 3 represent multilayer structures. Depending on the molecular orientation, film 2 may correspond to the adsorption of 2−4 layers, and film 3, 4−8 layers of histidine, respectively.

Besides the estimates of the film thicknesses, a careful analysis of Au 4f core-level spectra reveals important information on the strength of the adsorbate−substrate interactions. Both components of the Au 4f spin−orbit doublet in the spectrum of clean, freshly sputtered gold ($4f_{5/2}$ and $4f_{7/2}$) exhibit (see Figure 4) asymmetric shapes due to the overlap of the contributions related to the bulk (83.98 eV for Au $4f_{7/2}$) and surface (83.58 eV) of the gold substrate.[33]

In the case of film 1, the surface component is entirely suppressed and a new component emerges with a binding energy more than 1 eV higher than the former surface component (84.66 eV). This "shift" clearly indicates that the gold atoms at the interface experience a very different electronic and/or chemical environment, for example, by acquiring a partial positive charge upon the adsorption of the histidine monolayer. This is reasonable, assuming that the chemical form of adsorbed histidine is most probably anionic and that the bonding is strong and essentially ionic−covalent (as opposed to a van der Waals type bonding). The absence of the (unshifted) surface component indicates nearly complete coverage. In combination with the aforementioned thickness estimate, this finding gives evidence that film 1 corresponds to approximately one full monolayer of histidine on the gold substrate.

For films 2 and 3, the shift in the binding energy of the interface component is much smaller than for film 1: it amounts to ca. 0.35 eV with respect to the surface peak of clean gold and hence overlaps with the bulk peak. This implies that adsorption of the second, third, and further layers of histidine alters the electronic and/or chemical environment of the interfacial Au atoms, by strong intermolecular interactions within the adsorbed layer and/or by an alteration of the final state of the photoemission process (e.g., screening of the photohole on the femtosecond time scale). It appears that, upon adsorption of the multilayers, the bond between the monolayer and the Au surface is substantially weakened, most likely due to strong Coulomb interactions within the organic layer.

More details on the chemical form of adsorbed histidine molecules and adsorbate−substrate bonding in films 1−3 can be gained from an analysis of the C 1s, N 1s, and O 1s core-level spectra. The O 1s core-level spectra are shown in the second panel of Figure 4. The spectra of films 2 and 3 are quite similar: they can be fitted with one dominant spectral component at ca. 531.8 eV (B) and a minor component, shifted by about 1.1 eV toward higher binding energy (BE) (A). This panel of Figure 4 also shows a spectrum of histidine measured on a polycrystalline powder sample by use of a laboratory XPS spectrometer. It also exhibits one dominant component, though significantly broadened due to the poorer instrumental resolution. The major component B is attributed to the equivalent oxygen atoms in zwitterionic histidine. The minor component A corresponds either to a shake-up satellite of the major peak or to the hydroxyl oxygen of the protonated carboxyl group, which is characteristic of neutral histidine. On the basis of the relative intensity of this minor component, the fraction of neutral molecules in the multilayers is estimated to be at most 20−30%. We hence conclude that histidine molecules in the bulk of the film are predominantly zwitterionic, whereas neutral molecules may be present at the histidine−vacuum interface or at defect sites. A small shift of both components to higher BE by 0.2 eV upon going from film 2 to film 3 is attributed to final state screening, which is more efficient in the thinner film 2.

For monolayer film 1, the O 1s spectrum is distinctly different from those of the two multilayer films (see Figure 4). Assuming the same full width at half-maximum (fwhm) of individual spectral components as for films 2 and 3 (1.25 eV according to the peak fitting analysis), at least three bands are required to achieve a good fit to the experimental data. This indicates the presence of at least two chemically different histidine species in the monolayer film. Note that the spectrum exhibits no significant contribution from component A (hydroxyl oxygen), corroborating that the carboxyl groups are predominantly not protonated. Additionally, component B can be fitted with two subcomponents with a separation of 0.7 eV. And a new component, denoted C, at a significantly lower BE of 530.2 eV is apparent. We attribute feature C to a carboxylate group ($-COO^-$) oxygen atom coordinated to gold. The lower BE is most probably due to a much better (e.g., charge transfer) screening of the coordinated oxygen atom by the Au substrate electrons. Moreover, the negative charge of the carboxylate may

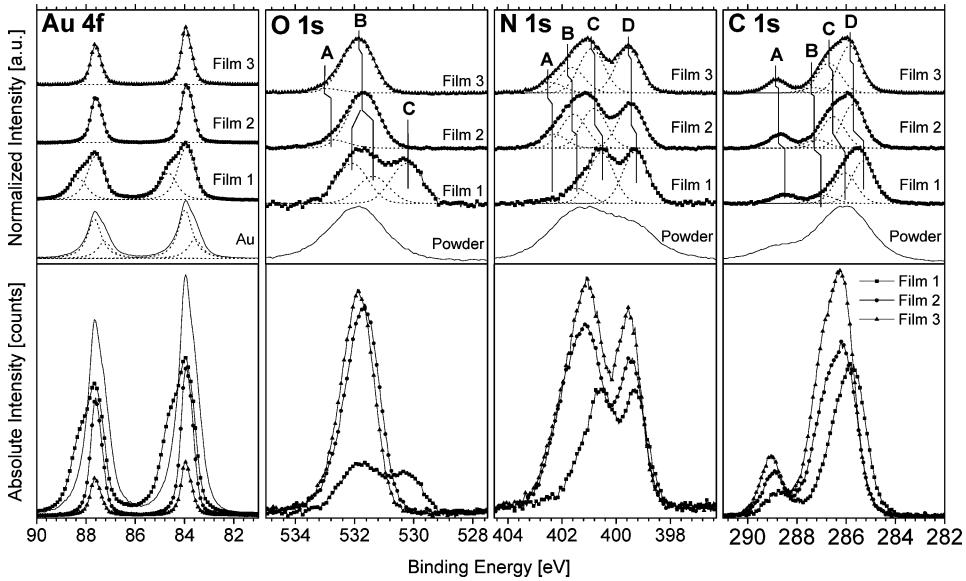

Figure 4. Top row (from left to right): Au 4f, O 1s, N 1s, and C 1s core-level spectra ($h\nu = 610$ eV) for histidine films 1−3 and freshly sputtered gold (Au 4f) or histidine powder (O 1s, N 1s, and C 1s), normalized to the maximum intensity. Dotted lines show peak-fitting results. Bottom row: identical spectra but normalized to the storage ring current.

be localized on this low-BE C oxygen atom (rather than delocalized over two atoms as in an uncoordinated carboxylate), contributing to the observed spectral shift. The higher-BE subcomponent of peak B with an intensity equal to that of component C is then assigned to the keto oxygen of the coordinated carboxylate. The lower-BE subcomponent of peak B is assigned to two equivalent oxygen atoms of uncoordinated or symmetrically coordinated carboxylates with delocalized charge. On the basis of the intensity ratios of the respective spectral features, the fraction of asymmetrically coordinated carboxylates is estimated to be about 70%.

The N 1s spectra for multilayer films 2 and 3, as shown in the third panel of Figure 4, are similar to each other and to a spectrum of histidine powder recorded at a poorer resolution. This observation is in agreement with the predominance of zwitterions in the bulk of the histidine samples. The N 1s spectra have complicated shapes. An adequate peak fit can be achieved by use of four components with equal fwhm of 1.1 eV, denoted A−D in Figure 4. It is generally assumed that the preferable protonation site for the histidine zwitterion is the amino group. In particular, zwitterions with protonated amino groups were found in single crystals of pure histidine by means of X-ray diffraction.[34] However, protonation of the imidazole ring could also take place. For instance, cationic histidine species (His + $H)^+$ are, according to the acid−base equilibria shown in Figure 2, the dominant dissolved species of histidine at neutral pH. They can be stabilized in the solid state in molecular complexes of histidine even with very weak acids, such as aspartic acid.[35] Moreover, protonation of the imidazole ring was found to be energetically favorable with respect to the amino group for gaseous histamine (which is, essentially, histidine without the carboxyl group).[36,37] Thus, a partial delocalization of the positive charge over two H^+-acceptor sites[38] cannot be ruled out when the spectra are analyzed. This makes unambiguous assignment of the features in the N 1s XPS spectra to chemically nonequivalent nitrogen atoms impossible. We propose that the two lower-BE features (C and D in Figure 4) correspond to formally neutral N atoms, with the N_3 atom predominantly contributing to the D feature (399.5 eV) and the N_1 atom, together with the amino group, contributing to the C feature (400.9 eV). Correspondingly, the two higher-BE components A (402.4 eV) and B (401.6 eV) are expected to be due to protonated nitrogen atoms of the amino groups and the imidazole rings, respectively. Note that in glycine adsorbed on Pt(111), the N 1s XPS signal of protonated amino groups was found at ca. 402.5 eV as compared to the neutral amino groups at ca. 400.5 eV.[12] Adopting this interpretation, the fraction of zwitterionic histidine in multilayer films is estimated to be 60−75%, in reasonable agreement with the aforementioned estimate from the O 1s data. Note, however, that the interpretation assumes that two different types of histidine zwitterions with protonated amino groups and imidazole rings are present in the films in similar proportions and that satellite features do not play a significant role in the N 1s spectra.

The N 1s spectrum for film 1 is again dramatically different from the multilayer spectra (see third panel of Figure 4). Apart from a general shift of the spectrum toward lower BE, which may be caused by the above-mentioned final-state-screening effects, the relative intensities of components B and, especially, A are substantially reduced. Within the proposed assignment, this means that the protonation degree of histidine decreases from 60−75% to ca. 20% (15% from protonated imidazole rings and 5% from protonated amino groups) with decreasing film thickness. This, together with the Au 4f and O 1s data discussed above, gives strong evidence that histidine molecules in the monolayer film 1 are predominantly anionic. A minor fraction of zwitterionic histidine is likely also present.

C 1s core-level spectra of films 1−3 are shown in the fourth panel of Figure 4, along with the low-resolution spectrum measured on a polycrystalline powder. In the case of C 1s, a strict assignment of the spectral features is even more ambiguous than for N 1s since, already in the neutral histidine, there are six chemically nonequivalent carbon atoms. Assuming that carbon atoms are not strongly involved in a redistribution of charges upon zwitterion formation, we adopt the following assignment of the spectral features: A (288.8 eV), carboxylic carbon; B (287.3 eV), satellite; C (286.7), C_2 and C_α; D (285.8), C_5, C_β, and C_4. The difference between the spectra of films 2 and 3 on one side and film 1 on the other is not as dramatic as in the case of oxygen and nitrogen: the general spectral shape is retained and only a shift of 0.3−0.4 eV toward lower BE is observed for film 1. This shift may be explained by a net

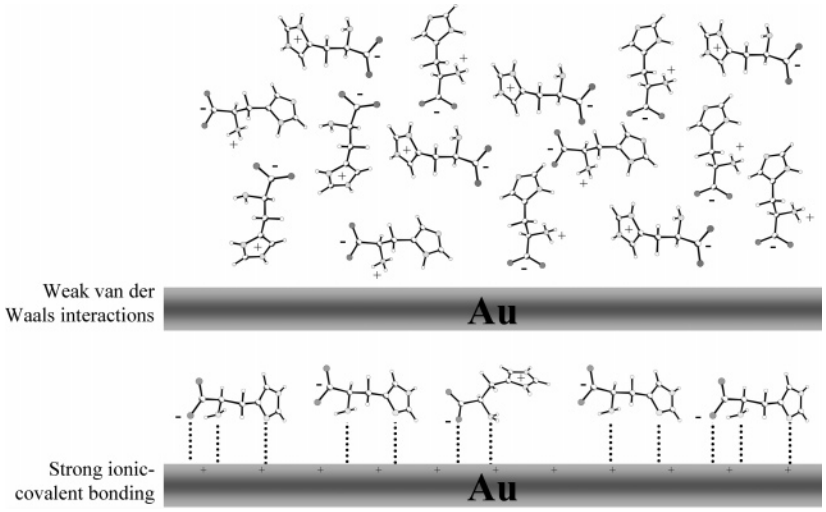

Figure 5. Models for the adsorption of histidine on polycrystalline gold in the monolayer (bottom) and multilayer (top) regimes.

negative charge of the adsorbed histidine species or by final-state-screening effects.

The obvious similarity between the XPS spectra of vacuum-deposited multilayer films and of polycrystalline powder of histidine demonstrates that only intact histidine molecules are adsorbed. The multilayers most probably represent three-dimensional aggregates of randomly oriented histidine molecules, strongly interacting with each other via Coulomb forces (e.g., between charged sites of zwitterions) and/or H-bonding, and only weakly bound to the substrate via van der Waals forces as shown schematically in the top panel of Figure 5.

In contrast, in the monolayer regime (film 1), histidine is adsorbed in the anionic form, which is strongly coordinated to the gold substrate. A stabilization of the nonprotonated state of the amino group and the N_3 atom of the imidazole ring may be achieved by coordination to gold atoms. We suggest that both coordinatively active N-sites contribute to the histidine−substrate bonding, in addition to the carboxyl groups. This may be realized either by a tridentate coordination of histidine or by several bidentate coordination types as schematically depicted in the bottom panel of Figure 5.

The finding of a very different interface bonding between Au and the first histidine layer depending on film thickness is rather unexpected and may have far-reaching implications. These will be addressed when answers to some of the open questions are experimentally found such as the molecular orientation in mono- and multilayers. Another interesting question that also cannot be answered by the present experiments is, does the strong ionic−covalent interface bonding already develop during adsorption of the first layer and is then changed upon adsorption of further histidine layers due to strong intermolecular interaction, or does it develop only for an isolated monolayer, perhaps involving certain adsorption sites, or molecular orientations, or even an activation barrier which may cause a delayed bond formation? Yet another open question that closely relates to the above ones concerns behavior of hydrogen atoms. The presence of histidinate anions in the monolayer implies that the neutral histidine molecules undergo deprotonation on the Au surface. It is widely accepted that hydrogen does not form sufficiently stable adsorbates on a clean gold surface[39] and thus it would be logical to expect that the histidine deposition is accompanied by liberation of molecular hydrogen. Nevertheless, taking into account that histidinate anions induce a serious change in the chemical state of the topmost layer of gold atoms, we cannot totally rule out that some hydrogen atoms appear weakly bound to the surface. More studies involving supplementary experimental techniques (in particular, IR spectroscopy) and, probably, other metal substrates (e.g., Cu, Ni, etc.) are needed to clarify the situation.

3.2. Radiation-Induced Decomposition of Histidine Films. Amino acids readily decompose under prolonged or intense soft X-ray irradiation.[30] To monitor small changes in the chemical state of amino acids (e.g., due to water adsorption, as discussed below) by soft X-ray spectroscopies utilizing very intense radiation of the third-generation synchrotron sources, it is important to know the dominant decomposition pathways and to have estimates of the respective rates. For this purpose, a series of dedicated measurements was performed on the histidine multilayer film 2. Note that such ultrathin films are especially suitable for studies of radiation damage by XPS since changes in the absolute intensity of different XPS lines may be quantified and associated with specific mass losses, whereas only relative changes are detectable in studies of powder samples.

Changes in the shapes of the N 1s, C 1s, and O 1s XPS spectral lines for film 2, exposed to soft X-ray radiation at $h\nu = 610$ eV for an equivalent time of 25 min, are shown in Figure 6 (normalized to maximum intensity). The time-dependent changes in absolute intensities with respect to the pristine state are plotted in Figure 7. Distinct changes in the line shapes are observed in the N 1s spectrum. Qualitatively, they may be described as a relative gain in intensity of components C and D, at the costs of A and B (see left panel of Figure 6). Yet this change is not associated with any significant nitrogen loss; that is, the absolute intensity of the N 1s signal remains constant within the experimental accuracy during the radiation exposure (see Figure 7). Hence, this change can be interpreted as a manifestation of the intra- or intermolecular proton transfer, resulting in a deprotonation of imidazole rings and amino groups of the zwitterionic histidine. Such a conversion of zwitterionic amino acids into neutral molecules has been established earlier as one of the dominant processes initiated by soft X-ray irradiation.[30]

The only change detectable in the C 1s spectrum (central panel of Figure 6) is a pronounced drop in the relative intensity of component A, which is assigned to carbon atoms of the carboxylic groups. Similarly, the absolute intensity of this component decreases progressively during irradiation while the integral intensity of the C 1s signal changes insignificantly (see Figure 7). Therefore, the only important pathway of the radiation-induced carbon loss is the decarboxylation of histidine.

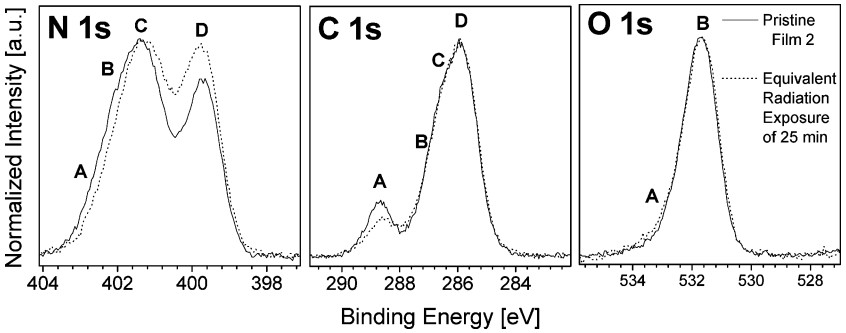

Figure 6. Relative changes in the N 1s, C 1s, and O 1s spectra due to exposure of histidine film 2 to soft X-ray radiation at $h\nu = 610$ eV.

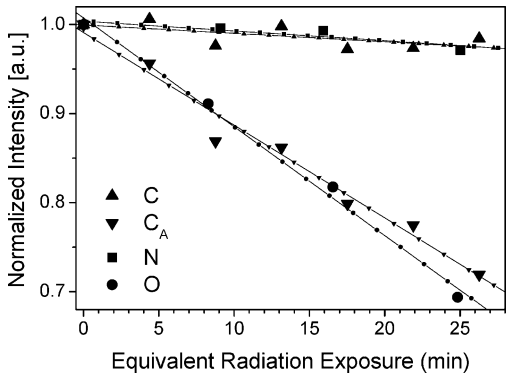

Figure 7. Relative changes of the integrated signal intensities during soft X-ray irradiation of histidine film 2. In addition, the development of peak A in the C 1s spectrum is plotted.

Changes associated with the O 1s line give further evidence that the decarboxylation is the dominant pathway of histidine radiation-induced decomposition. Indeed, as shown in the right panel of Figure 6, the O 1s line profile does not change much due to irradiation, whereas the absolute intensity of the O 1s signal decreases in parallel to that of the carboxylic carbon (C_A).

Thus, radiation exposure of the histidine film results in a partial mass loss, that is, in a radiation-induced "evaporation" of functional groups from the organic overlayer (this can be seen also from the survey XPS spectra shown in Figure 3). An analysis of the absolute intensities of the Au 4f lines indicates that the effective thickness of film 2 decreases from 18.5 to 14.8 Å as a result of the equivalent radiation exposure of ca. 30 min. This change is caused predominantly by the loss of oxygen and carbon through decarboxylation of histidine, suggesting that the sample is enriched with histamine-like species. Additionally, the zwitterion/neutral molecule ratio is noticeably affected by the irradiation. Nevertheless, we note that the radiation damage under the present conditions is reasonably slow: statistically significant spectral changes are observed only after 5−10 min of radiation exposure. Therefore, radiation effects are nearly negligible on the time scale of a single XPS scan (normally less than 2 min). This means that the results presented in sections 3.1 and 3.2 are indeed representative for the pristine histidine films.

3.3. Adsorption of Water on Histidine Films. According to the scheme of histidine acid−base equilibria shown in Figure 2, aqueous solutions of histidine at neutral and weakly basic pH contain ionic species of two major types, zwitterions (ZI) and cations (His + H^+). However, in crystalline histidine, no potential counteranions are present, and therefore only zwitterions are found. Thus, it is expected that adsorption of water on a histidine film may influence the charge state of the histidine molecules.

A survey XPS spectrum of histidine multilayer film 3 kept at 100 K in UHV for about 200 min is shown in Figure 3. When the peak widths are taken into account, it is clearly seen that, upon this treatment, the O 1s line gains in intensity with respect to the other lines. We attribute this change to adsorption of water, which was the dominant component of the residual gas. The changes in the O 1s spectra of film 3 induced by water adsorption are shown in detail in Figure 8. A new component at ca. 534.0 eV (denoted W) and an increase in the relative intensity of component A are observed. A BE value of 534 eV is typical of molecularly adsorbed water.[40,41] For water−metal adsorbate systems (especially for active metals), the O 1s XPS peak of molecularly adsorbed water is often accompanied by another component shifted by 1.0−2.0 eV toward lower BE, which is attributed to hydroxyl anions.[40,41] Note, however, that water molecules tend to be involved in extended networks of hydrogen bonds, and thus a differentiation between a fully deprotonated and a strongly H-donating H_2O is ambiguous. Therefore, although component A was assigned in pristine histidine films 2 and 3 to hydroxyl groups of protonated carboxyls (assuming that a minor fraction of neutral histidine molecules is present), it may also be due to dissociatively adsorbed water. This allows a quantification of the water uptake as plotted in the right panel of Figure 8, which also shows the estimated water exposure in Langmuirs. For the maximum exposure time of ca. 200 min, the dose is approximately 3.6 Langmuirs, and the number of adsorbed water molecules is estimated to be twice the number of histidine molecules in the film.

Note that no systematic variations in absolute intensities were found for the Au 4f, C 1s, and N 1s lines. This indicates that adsorbed water most likely diffuses into the bulk of the film rather than forming a uniform ice layer, which would increase the effective film thickness. Furthermore, the shape of the Au 4f line is not altered by water adsorption, suggesting that the dissociation of water molecules is most likely not induced by the substrate. Further evidence for this model is given by the N 1s and C 1s XPS spectra shown in Figure 9. The change in the N 1s spectrum shown in the left panel of Figure 9 reveals a relative increase of the intensities of components A and B at the cost of C and D, indicating an increase in the degree of protonation in the histidine layer. Note that radiation damage would alter the spectra in the opposite direction, such that the effects can be easily differentiated. The shape of the carbon spectra (see central panel of Figure 9) is not changed significantly by water adsorption, although a general shift toward higher BE by ∼0.2 eV is consistent with a partial protonation of histidine molecules (assuming that carbon atoms are partly involved in a redistribution of the extra positive charge). Therefore, the XPS data show that adsorption of water onto histidine films is to some extent dissociative: adsorbed water molecules are capable of protonating histidine and forming hydroxyl anions.

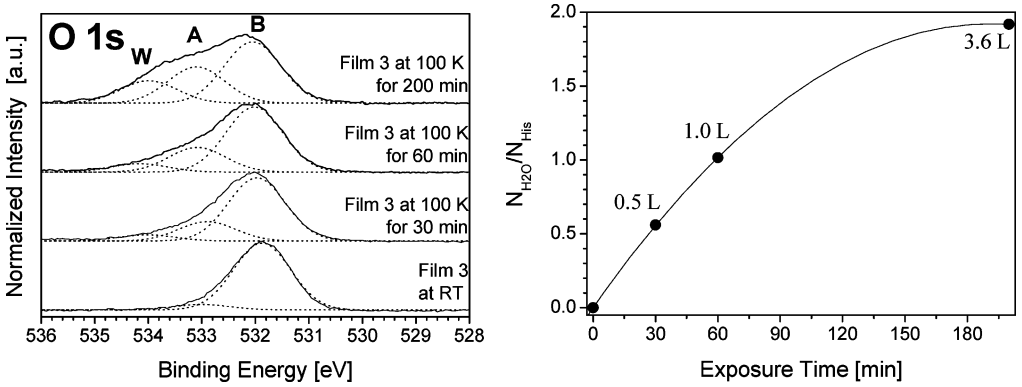

Figure 8. (Left) Changes in the O 1s spectra of histidine film 3 due to adsorption of water. (Right) Estimates of water uptake from the relative intensities of features A, B, and W in the O 1s spectra in the left panel. Numbers denote the estimated water exposure doses in Langmuirs (1 Langmuir = 10^{-6} Torr·s).

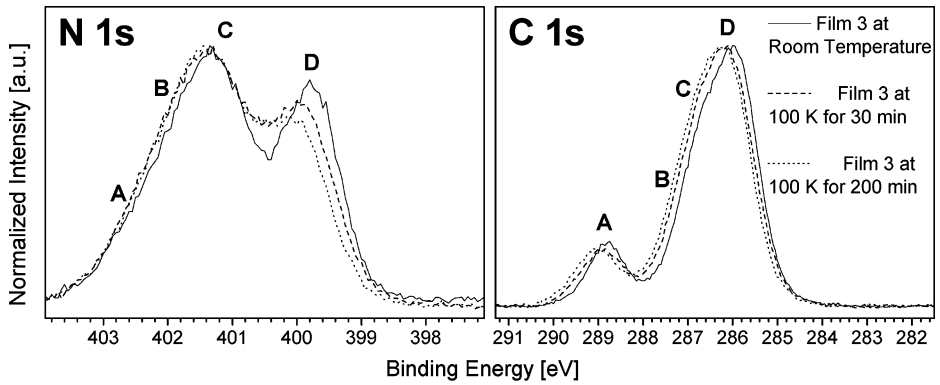

Figure 9. Changes in the N 1s and C 1s spectra of histidine film 3 due to adsorption of water.

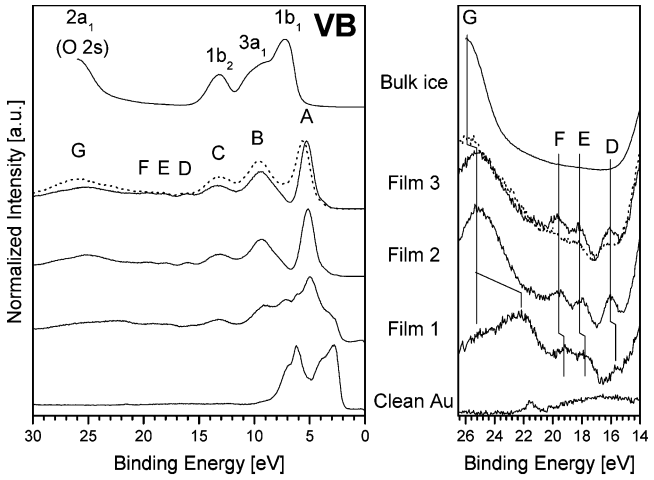

Figure 10. (Left) Valence band spectra of clean gold, pristine histidine films 1−3, histidine film 3 with adsorbed water (dotted line), and bulk ice ($h\nu$ = 160 eV). (Right) Enlarged region of the lower valence band (arbitrary magnification factors).

Valence-band spectra ($h\nu$ = 160 eV) of pristine histidine films 1−3 and of film 3 with adsorbed water are shown in Figure 10, along with the reference spectra of clean gold and bulk ice. To our knowledge, no valence-band UPS spectra of histidine have been reported so far. The spectra for multilayer films 2 and 3 are very similar to each other: they show seven basic emission lines labeled A−G and no features due to the substrate (in the spectrum of clean gold, peaks attributable to Au 5d-derived states are found at 2.8, 3.9, 6.2, and 7.0 eV). This again confirms the homogeneity of the deposited films. Peak A at ca. 5.2 eV may be assigned to photoemission from several nonbonding orbitals near the highest occupied molecular orbital (HOMO) of histidine, localized on the nitrogen (amino group and N_3 of the imidazole ring) and oxygen atoms (lone pairs). Features B (9.5 eV) and C (13.2 eV) originate from strongly delocalized bonding molecular orbitals of π and σ symmetry. Weak lines in the lower-valence band region, D (16.0 eV), E (17.9 eV), and F (19.6 eV) (this region is enlarged in the right panel of Figure 10), contain a substantial contribution of partly bonding C 2s states. The broad and relatively strong feature G (ca. 25.2 eV) is due to mostly localized O and N 2s states.

The valence-band spectrum of monolayer film 1 reveals a substantial contribution from the substrate. Despite the strong overlap with the Au 5d lines, features A and B of histidine are clearly resolvable, though a detailed analysis of their shapes is impossible. Other peaks C−G are also present in the spectrum. Note, however, that the relative intensity of the feature D is strongly reduced (see right panel). Moreover, feature G is split and its dominant component is shifted toward lower BE by ca. 3 eV. This change indicates a charge redistribution involving N and O atoms within the histidine molecules. This observation is in accord with the above-proposed anionic character of adsorbed histidine molecules in monolayer film 1.

Several changes in the spectrum of film 3 due to water adsorption (dotted line in Figure 10) are worth noting. First of all, the intensities of features B and C are enhanced. This is not surprising since in the valence-band spectrum of bulk ice (top curve in Figure 10) emission lines from $3a_1$ and $1b_2$ molecular orbitals (with bonding σ_{O-H} character) are observed at similar BE, that is, at ca. 9.5 and 13.2 eV, respectively. Note that no distinct maximum at 7.2 eV emerges, which is the dominant feature in bulk ice associated with photoemission from the nonbonding $1b_1$ orbital (oxygen lone pair). Instead, the shape of peak A slightly changes so that its spectral maximum shifts by 0.3 eV to higher BE. This indicates that the adsorbed water

molecules do not form a separate icelike phase but rather directly interact with the histidine molecules. Finally, peak G also increases in relative intensity and shifts toward higher BE by ~0.6 eV due to an increased contribution of the O 2s states of water.

4. Conclusions

We described the experimental conditions for the successful vacuum deposition of thin histidine films on polycrystalline gold in mono- and multilayer regimes.

In monolayer films, histidine is adsorbed on the surface of polycrystalline gold as histidinate anions forming strong ionic−covalent bonds with the gold substrate atoms (which acquire a partial positive charge). Amino groups, N_3 atoms of imidazole rings, and carboxylate groups are probably involved in the bonding to the substrate. Carboxylate groups are coordinated asymmetrically, that is, via one of the two oxygen atoms. The spectroscopic data do not allow an unambiguous differentiation between possible bi- and tridentate coordination types.

In the multilayer film, histidine molecules are predominantly zwitterionic. They form 3D aggregates bound by strong intermolecular forces and only weakly interact with the substrate. Two types of zwitterions, viz., with protonated amino groups and with protonated imidazole rings, are present in the multilayer film in about equal proportions.

We find that soft X-ray irradiation of the histidine multilayer film induces a discharge of zwitterions to form neutral molecules and a mass loss via decarboxylation.

Water is dissolved in the multilayer histidine film and partly dissociated, producing hydroxyl anions and increasing the degree of protonation of the histidine molecules.

Acknowledgment. We are grateful to Dr. Th. Schmidt (University of Würzburg) for technical assistance during the experimental data collection. This work was supported by the German BMBF (Projects 05 KS1VHA/3 and 05 KS1WW1/6), the Fonds der Chemischen Industrie (M.G. and E.U.), and the Austrian Science Foundation (G.T. and F.P.N). We are also grateful to the BESSY staff for their technical support.

References and Notes

(1) Kasemo, B. *Curr. Opin. Solid State Mater. Sci.* **1998**, *3*, 451.
(2) Uvdal, K.; Bodoe, P.; Liedberg, B. *J. Colloid Interface Sci.* **1992**, *149*, 162.
(3) Ihs, A.; Liedberg, B.; Uvdal, K.; Toernkvist, C.; Bodoe, P.; Lundstroem, I. *J. Colloid Interface Sci.* **1990**, *140*, 192.
(4) Liedberg, B.; Carlsson, C.; Lundstroem, I. *J. Colloid Interface Sci.* **1987**, *120*, 64.
(5) Liedberg, B.; Lundstroem, I.; Wu, C. R.; Salaneck, W. R. *J. Colloid Interface Sci.* **1985**, *108*, 123.
(6) Liedberg, B.; Ivarsson, B.; Lundstroem, I.; Salaneck, W. R. *Prog. Colloid Polym. Sci.* **1985**, *70*, 67.
(7) Williams, J.; Haq, S.; Raval, R. *Surf. Sci.* **1996**, *368*, 303.
(8) Barlow, S. M.; Kitching, K. J.; Haq, S.; Richardson, N. V. *Surf. Sci.* **1998**, *401*, 322.
(9) Booth, N. A.; Woodruff, D. P.; Schaff, O.; Giessel, T.; Lindsay, R.; Baumgärtel, P.; Bradshaw, A. M. *Surf. Sci.* **1998**, *397*, 258.
(10) Hasselström, J.; Karis, O.; Weinelt, M.; Wassdahl, N.; Nilsson, A.; Nyberg, M.; Pettersson, L. G. M.; Samant, M. G.; Stöhr, J. *Surf. Sci.* **1998**, *407*, 221.
(11) Hasselström, J.; Karis, O.; Nyberg, M.; Pettersson, L. G. M.; Weinelt, M.; Wassdahl, N.; Nilsson, A. *J. Phys. Chem. B* **2000**, *104*, 11480.
(12) Löfgren, P.; Krozer, A.; Lausmaa, J.; Kasemo, B. *Surf. Sci.* **1997**, *370*, 277.
(13) Benninghoven, A.; Kempken, M.; Kluesener, P. *Surf. Sci.* **1998**, *206*, L927.
(14) Holtkamp, D.; Kempken, M.; Kluesener, P.; Benninghoven, A. *J. Vac. Sci. Technol. A* **1987**, *5*, 2912.
(15) Holtkamp, D.; Lange, W.; Jirikowsky, M.; Benninghoven, A. *Appl. Surf. Sci.* **1984**, *17*, 296.
(16) Henry, B.; Tekely, P.; Delpuech, J.-J. *J. Am. Chem. Soc.* **2002**, *124*, 2025.
(17) Munowitz, M.; Bachovchin, W. W.; Herzfeld, J.; Dobson, C. M.; Griffin, R. G. *J. Am. Chem. Soc.* **1982**, *104*, 1192.
(18) Sundberg, R. J.; Martin, R. B. *Chem. Rev.* **1974**, *74*, 471.
(19) Krogh-Jespersen, K.; Westbrook, J. D.; Potenza, J. A.; Schugar, H. J. *J. Am. Chem. Soc.* **1987**, *109*, 7025.
(20) Evertsson, B. *Acta Crystallogr. B* **1969**, *25*, 30.
(21) Baidina, I. A.; Slyudkin, O. P.; Borisov, S. V. *Zh. Strukt. Khim.* **1990**, *31*, 144.
(22) Czernuszewicz, R. S.; Yan, Q.; Bond, M. R.; Carrano, C. J. *Inorg. Chem.* **1994**, *33*, 6116.
(23) Cuadrado, J. A.; Zhang, W.; Hang, W.; Majidi, V. *J. Environ. Monitor.* **2000**, *2*, 355.
(24) Khudyakova, R. V.; Soloshko, S. V.; Safronov, A. Y. *Russ. J. Electrochem.* **1997**, *33*, 1081.
(25) Wienkea, M.; Lippert, B.; Zangrando, E.; Randaccio, L. *Inorg. Chem.* **1992**, *31*, 1983.
(26) Zou, J.; Taylor, P.; Dornan, J.; Robinson, S. P.; Walkinshaw, M. D.; Sadler, P. J. *Angew. Chem., Int. Ed.* **2000**, *39*, 2931.
(27) Liedberg, B.; Carlsson, C.; Lundstroem, I. *J. Colloid Interface Sci.* **1987**, *120*, 64.
(28) Arnold, F. H. *Bio/Technology* **1991**, *9*, 151.
(29) Kroger, D.; Liley, M.; Schiwek, W.; Skerra, A.; Vogel, H. *Biosens. Bioelectron.* **1999**, *14*, 155.
(30) Zubavichus, Y.; Fuchs, O.; Weinhardt, L.; Heske, C.; Umbach, E.; Denlinger, J. D.; Grunze, M. *Radiat. Res.* **2004**, *161*, 346.
(31) Laibinis, P. E.; Bain, C. D.; Whitesides, G. M. *J. Phys. Chem.* **1991**, *95*, 7017.
(32) Harder, P.; Dahint, R.; Grunze, M.; Witesides, G. M.; Laibinis, P. E. *J. Phys. Chem. B* **1998**, *102*, 426.
(33) Heister, K.; Zharnikov, M.; Grunze, M.; Johansson, L. S. O. *J. Phys. Chem. B* **2001**, *105*, 4058.
(34) Coppens, P.; Abramov, Y.; Carducci, M.; Korjov, B.; Novozhilova, I.; Alhambra, C.; Pressprich, M. R. *J. Am. Chem. Soc.* **1999**, *121*, 2585.
(35) Bhat, T. N.; Vijayan, M. *Acta Crystallogr. B* **1978**, *34*, 2556.
(36) Hernández-Laguna, A.; Abboud, J.-L. M.; Notario, R.; Homan, H.; Smeyers, Y. G. *J. Am. Chem. Soc.* **1993**, *115*, 1450.
(37) Darowska, M.; Raczynska, E. D. *Pol. J. Chem.* **2002**, *76*, 1027.
(38) Elvidge, J. A.; Jones, J. R.; Salih, R.; Shandala, M.; Taylor, S. E. *J. Chem. Soc., Perkin Trans. 2* **1980**, *2*, 447.
(39) Hammer, B.; Norskov, J. K. *Nature* **1995**, *376*, 238.
(40) Thiel, P. A.; Madey, T. *Surf. Sci. Rep.* **1987**, *7*, 211.
(41) Henderson, M. *Surf. Sci. Rep.* **2002**, *46*, 1.